Interseismic Coupling, Megathrust Earthquakes and Seismic Swarms Along the Chilean Subduction Zone (38A degrees-18A degrees S)

Marianne Metois, C. Vigny, A. Socquet

Interseismic coupling, megathrust earthquakes and seismic swarms along the Chilean subduction zone (38°-18°S)

M. Métois*, C. Vigny†, A. Socquet‡

March 16, 2016

Abstract

The recent expansion of dense GPS networks over plate boundaries allows for remarkably precise mapping of interseismic coupling along active faults. The interseismic coupling coefficient is related to the ratio between slipping velocity on the fault during the interseismic period and the long-term plates velocity, but the interpretation of coupling in terms of mechanical behaviour of the fault is still unclear. Here, we investigate the link between coupling and seismicity over the Chilean subduction zone that ruptured three times in the last 5 years with major earthquakes (Maule Mw 8.8 in 2010, Iquique Mw 8.1 in 2014 and Illapel

*Université Claude Bernard Lyon 1 LGLTPE-Osu de Lyon Bâtiment Géode, Campus La Doua UMR (marianne.metois@univ-lyon1.fr)

†Laboratoire de Géologie, Ecole normale supérieure Paris, France

‡Université Joseph Fourier, Institut des Sciences de la Terre Grenoble, France

Mw 8.4 in 2015). We combine recent GPS data acquired over the margin (38°-18°S) with older data to get the first nearly continuous picture of the interseismic coupling variations on the subduction interface. Here, we show that at least six low coupling zones (LCZ), areas where coupling is low relatively to the neighboring highly coupled segments can be identified. We also find that for the 3 most recent Mw>8 events, co-seismic asperities correlate well with highly coupled segments, while LCZ behaved as barriers and stopped the ruptures. The relation between coupling and background seismicity in the interseismic period before the events is less clear. However, we note that swarm sequences are prone to occur in intermediate coupling areas at the transition between LCZ and neighboring segments, and that the background seismicity tends to concentrate on the downdip part of the seismogenic locked zone. Thus, highly coupled segments usually exhibit low background seismicity. In this overall context, the Metropolitan segment that partly ruptured during the 2015 Illapel earthquake appears as an outlier since both coupling and background seismicity were high before the rupture, raising the issue of the remaining seismic hazard in this very densely populated area.

1 Introduction

GPS instrumentation along active plate boundaries has contributed significantly to better constrain the characteristics and mechanics of large destructive megathrust earthquakes. For instance,the coseismic slip of the Mw 8.8 2010 Maule earthquake that ruptured the South-Central part of the Chilean subduction zone has been precisely imaged using GPS data from local campaign networks installed since the early 90's in the epicentral region (e.g RUEGG et al., 2009;

MORENO et al., 2010; MÉTOIS et al., 2012). The deformation of the sea floor off the Sendai coast measured by offshore geodesy brought unique insights on the shallow slip during the Tohoku Mw 9 2011 earthquake (e.g SIMONS et al., 2011; SATO et al., 2011). Moreover, analysis of the seismicity or cGPS time-series before the 2011 Tohoku and the 2014 Mw 8.2 Iquique earthquakes show that anomalous activity was going on in the vicinity of these megathrust earthquakes, days or weeks before the rupture itself (e.g. KATO et al., 2012; RUIZ et al., 2014; SCHURR et al., 2014). Seismic and tsunami records have shown that the 2015 Mw 8.4 Illapel earthquake ruptured a shallow portion of the subduction zone (YE et al., 2015; ÁRANGUIZ et al., 2016; CALISTO et al., 2016), while GPS measurements conducted after the 2010 Maule earthquake show that the 2015 rupture area was affected by eastward postseismic motion, suggesting an indirect trigerring between the Maule and Illapel earthquakes (RUIZ et al., 2016; KLEIN et al., 2016). Overall, the present day challenge for the scientific community remains in the deep understanding of the mechanical behavior of the fault interface, that should help identify zones of high seismic hazard between highly coupled segments with low background seismicity, and more complex zones where precursory activity could develop before the occurrence of the next megathrust earthquake.

Over the last decades, geodetic measurements conducted during the interseismic phase along several subduction zones have provided maps of the upper-plate deformation that reflect the degree of locking between plates on the interface (e.g CHLIEH et al., 2008; WALLACE et al., 2004; LOVELESS and MEADE, 2011; MCCAFFREY, 2002; YOSHIOKA et al., 2005; MORENO et al., 2008; MCCAFFREY, 2014). However, these works often suffer from heterogeneous or sparse measurements and from the large distance between the coast and the trench (more than 200

57 km in Japan or Sumatra) that impede detailed mapping of the along-strike or along-dip variations
58 of the coupling coefficient. Furthermore, although there seems to be a good correlation between
59 interseismic coupling and seismic rupture in general (e.g. CHLIEH et al., 2008; KONCA et al.,
60 2008; MORENO et al., 2010; MÉTOIS et al., 2012; LOVELESS and MEADE, 2011; RUIZ et al.,
61 2016), how kinematic coupling relates with the mechanical properties of the interface and to the
62 shape and magnitude of the coming earthquakes are open questions that are still being actively
63 discussed (e.g MORENO et al., 2010; KANEKO et al., 2010; HETLAND and SIMONS, 2010).

64 The fast Nazca-South America convergence zone ($\sim$68 mm/yr (e.g. VIGNY et al., 2009; AR-
65 GUS et al., 2011)), where little partitioning occurs but that is seismically very active (one Mw$>$8
66 every ten years in average, but already three since 2010) is a suitable place to determine inter-
67 seismic coupling and to investigate its relation with mechanical properties of the interface and
68 characteristics of the upper and downgoing plates. In particular, because the distance between
69 the coast and the trench is smaller than elsewhere (around 100 km and up to 70 km locally), the
70 Chilean subduction zone is a good candidate for such study, because it allows a good resolution
71 almost up to the trench. Hence, we build for the first time a nearly continuous map of interseis-
72 mic coupling along this subduction zone (38°-18°S) that we compare with the slip distributions
73 of the 2010 (Maule), 2014 (Iquique) and 2015 (Illapel) Mw$>$8 megathrust earthquakes and with
74 the "background" seismicity, i.e. the moderate-magnitude earthquakes that occurred on the plate
75 interface before the main shocks.

2 Tectonic context

In the following, we consider the Chilean margin deformation at a very large scale, along a ∼3000 km long portion of the subduction between the Nazca and South American plates, from 38° to 18°S. Therefore, the margin's distinctive features (e.g. slab geometry, trench sedimentation style, nature and structure of the upper and downgoing plates, volcanic activity) significantly vary from South to North in our study area (see (HOFFMANN-ROTHE et al., 2006) for a review). In particular, the Andean mountain belt resulting from the long-term deformation of South America is more than 450 km wide from 18°S to 26°S where it is characterized by the ∼3500 m high Altiplano-Puna plateau to the North and the Subandean active fold-and-thrust belt on its eastern front (Fig.1, (ARMIJO et al., 2010)). The main belt is less complex and is only 150 km wide south of 33°S, with no clear eastern front and no uplifted plateau. From 26° to 33°S in Central Chile, the principal cordillera is relatively sharp while the wide Sierras Pampeanas diffuse deformation area develops to the East with several active thrust fronts (e.g. REILINGER and KADINSKY-CADE, 1985; BROOKS et al., 2003).

The coastal cordillera is separated from the principal cordillera by the central valley in the North (18°-24°S) and South-Central Chile (32°-38°S). In South-Central Chile, the western front of the Andes has been described as an active crustal thrust (ARMIJO et al., 2010; VARGAS et al., 2014). Central Chile (24°-32°S) appears again as an outlier in this overall pattern since the transition from the coastal to principal cordillera is smooth, i.e. the central valley vanishes. This peculiar region overlays the deep Pampean flat-slab area where the Nazca plate flattens at ∼100 km depth and where no subduction-associated volcanism is observed (see Fig.1, TASSARA

et al., 2006; MAROT et al., 2014). Closer to the trench, we observe smaller scale (several tens of kilometers) variations of the Chilean coast morphology like large bays (e.g. La Serena or Baranquilla bays) and peninsulas (e.g. Arauco or Mejillones peninsula), the latter being often associated to complex crustal fault networks (e.g. MELNICK and BOOKHAGEN, 2009; ARMIJO and THIELE, 1990).

The Nazca plate characteristics also vary from North to South Chile : first, the subducted oceanic crust is younger in the South than in the North (45 Ma at 18°S and 28 Ma at 38°S (MULLER et al., 1997)) implying large differences in the thermal state of the lithosphere; second, the plate is deformed by volcanic ridges and fractures (high oceanic features or HOFs) with different orientations and wave lengths (Fig.1).

Besides all these lateral variations, the deformation of the entire region is dominated by the seismic cycle on the subduction interface that accommodates one of the highest convergent rates on Earth (68 mm/yr). As can be seen in Fig.2 where the moderate-size seismicity registered by the CSN (Centro Sismologico Nacional, *http://www.sismologia.cl/*) during the interseismic phase is plotted, the seismic activity illuminates the subduction interface down to 600 km depth, while only few earthquakes are recorded on shallow crustal structures. The exact amount of the Nazca-South America convergence that could be taken by these secondary active faults is still an open question, but it seems reasonable to assume that an overall 80 to 90% of the Chilean margin deformation is associated to the subduction fault from 38°S to 18°S. The 1 cm/yr velocity gradient observed across the subandean fold-and-thrust belt and its seismic activity led several authors to propose an Andean sliver independent from the South American craton that would absorb the remaining 10 to 20% relative motion (see Fig.1, KENDRICK et al., 2001; BROOKS

et al., 2003, 2011; CHLIEH et al., 2011; MÉTOIS et al., 2013, 2014; NOCQUET et al., 2014).

3 Interseismic velocity field

GPS measurements have been conducted by international teams in Chile since the early 90's both on survey and permanent networks (s- and c-GPS respectively), providing us with interseismic velocities measured over 20 years in some places (BEVIS et al., 2001; BROOKS et al., 2003, 2011; KHAZARADZE and KLOTZ, 2003; KLOTZ et al., 2001; RUEGG et al., 2009; VIGNY et al., 2009; BÉJAR-PIZARRO et al., 2009; CHLIEH et al., 2011). After the destructive 2010 Maule earthquake, a large instrumentation effort has been conducted over North and Central Chile (18-35°S) that provides us with unusually dense present-day measurements of interseismic loading on the interface over a 3 to 5-year time-span. Now, because of the 2 additionnal mega-thrust earthquakes of 2014 (Mw 8.1, Iquique) and 2015 (Mw 8.4, Illapel), that produced large co-seismic displacements and ongoing post-seismic deformation, it will not be possible to further refine the inter-seismic coupling in these aeas. Therefore, the data collected before these large earthquakes are the only way to understand the pre-existing strain and stress state of the Chilean interface to date.

We combine the data published by (RUEGG et al., 2009; MÉTOIS et al., 2013, 2014) to produce a consistent velocity field that homogeneously covers the 3000 km long portion of the plate boundary (18°-38°S), with the exception of a small gap in the Atacama desert area that still lacks measurements (24.3°-25.5°S). The resulting data set is formed of 248 recent horizontal GPS velocities that we combined together with most of the previously published data sets in

South-Central Chile (see MÉTOIS et al., 2012, for further details). We thus gather 396 horizontal velocities into a single data set (Fig.1) that we complete with 70 reliable vertical velocities (see supplementary figure 1).

This velocity field is heterogeneous since each data-set has been calculated on a different time-span : for instance, the interseismic velocities published by RUEGG et al. (2009) in the Maule area results from the 1996-2002 period, while the velocities published by MÉTOIS et al. (2013) in North Chile are derived from measurements made from 2008 to 2013. In order to remove from our data set velocities potentially affected by the 1960 earthquake postseismic motion still presently ongoing, we chose to exclude the velocities published by KLOTZ et al. (2001) south of 34°S and the velocities published by MORENO et al. (2008) south of 38°S in the 1960 epicentral area. Therefore, despite the fact that they are determined over different time windows, we are confident that all velocities presented in Fig.1 are "interseismic", i.e. are representative of the average deformation over several years before the occurrence of large ruptures on the megathrust interface.

The overall deformation pattern shown on Figure 1 relative to the stable South America as defined by NNR-Nuvel1A (DEMETS et al., 1994) is typical of the deformation expected from interseismic loading on a buried dislocation, at least at the first order (OKADA, 1985). Indeed, velocities are roughly parallel to the plate convergence in the near field, while they decrease and rotate towards a more trench perpendicular direction going inland and reach a null velocity in the South-American craton. Additional non-negligible north-eastward deformation ($\sim$1 cm/yr) is observed in the backarc, in particular in the Sierras Pampeanas and in the Altiplano Andes where only few mm per year should be observed in a purely elastic frame.

4 Modelling of GPS data

We use the Tdefnode code developed by McCaffrey (2009) based on backslip assumption and Okada's equations (Okada, 1985; Savage, 1983) to invert for the coupling distribution that best reproduces these data. We choose to simultaneously invert for the rigid rotation of an Andean sliver that would afford for part of the backarc deformation since it decreases significantly the normalized root mean square (nRMS) of the inversion and has been proposed by several previous works (Brooks et al., 2003; Métois et al., 2013; Nocquet et al., 2014). We present simpler 2-plate models for comparison in supplementary figures 5 and 7. Therefore, we assume that nearly all the observed deformation is elastic and due to the seismic cycle on the subduction interface, neglecting the small-scale deformation that could be produced by loading on second-order crustal faults (see section 2) but that is not detected by our regional campaign networks. For instance, the San Ramon active fault located at the edge of the Santiago basin is supposed to be loaded at 0.4 mm/yr (Armijo et al., 2010), a rate that is well beyond the s-GPS resolution. Similarly, the available data spanning the Sierras Pampeanas are too sparse to enable the detection of accumulation of elastic deformation on individual thrust faults. Therefore, we include this complex area in the South-American plate and consider the westernmost thrust front as the eastern boundary of the Andean sliver (Fig.1).

We divided the slab interface into a grid of 93 along-strike nodes (every 0.25°) and 11 along-dip nodes (every 7.5 km depth) based on the realistic Slab 1.0 geometry (Hayes et al., 2012). We use 862 independent observations to invert simultaneously for coupling on each nodes and the three parameters of the sliver Euler pole. To avoid numerical instabilities, we impose a 2D

(both along strike and dip) smoothing regularization that allows for the best compromise between small-scale coupling variations and fit to the data (*spread smoothing* technique proposed by McCaffrey, 2009). To limit the number of free parameters, we force the rake of the backslip component to be parallel to the plate convergence velocity.

We estimate the sensitivity of our data set to unit displacements on each node of the grid by summing the horizontal deformation on the whole network following Loveless and Meade (2011) (see supplementary figure 2 and checkerboard tests in supplementary figure 3). The "power" of our horizontal data to constrain the coupling on the interface is high from 15 km depth to more than 70 km depth in general. In areas where the measurements are very dense, i.e. from 33°S to 26°S, resolution is good nearly up to the trench. We lack resolution mainly on the edges of our model (in the Arica bend, and south of Arauco peninsula) and in the very shallow part of the subduction interface. Lack of measurements in the Taltal area (from 25°S to 26°S) makes the coupling unresolved in this region (see Fig.3-C). Recent instrumentation efforts should bring soon new clues about interseismic loading there. Based on this sensitivity test, it is important to note that coupling models are not -or barely- resolved in the first tens of kilometers of the slab. In other words, constraining the coupling value on these shallow nodes to either 0% or 100% does not impact the nRMS of the inversion. Therefore, using coupling models for generating tsunami scenarios that are mainly influenced by the shallow slip distribution is still challenging, even if promising results have been found for the Illapel earthquake where the coupling resolution is high even in the shallowest part of the slab (e.g. Calisto et al., 2016).

Our best coupling distribution (see Fig.3-C) reproduces well the data set with a nRMS around 1.6 for the horizontal velocities, and 2 for the vertical velocities. We find that the data require

a rotation motion of the Andean sliver around an Eulerian pole given by (56.37°S, 41.27°W, -0.12°/Myr) relative to stable South America (as defined by NNR-Nuvel1A (DeMets et al., 1994)) in close agreement with the pole determined in more local studies (Métois et al., 2013, 2014). This results in a ∼8 mm/yr translation-like motion of the Altiplano towards the North East in Northern Chile that decreases to less than 5 mm/yr in the backarc area of the Maule region where the subandean active front is no longer visible. If the Andean range is a rigid microplate, this would imply that a significant part of the Nazca-South America convergence is taken on the active subandean fold-and-thrust belt, reducing the total amount of potentially accumulated displacement on the subduction interface (Norabuena et al., 1998; Chlieh et al., 2011; Brooks et al., 2011).

5 Discussion

5.1 Kinematics of the Nazca-South America convergence

We model the surface deformation as a combination of elastic deformation coming from loading on the subduction interface and the rigid rotation of the so-called "Andean sliver" block. This modeling trick retrieves well the velocities observed in the Bolivian subandean fold and thrust belt (Brooks et al., 2011) and produces more realistic coupling distribution than a simpler 2-plate model since ~~then~~ no or little coupling is needed deeper than 60 km depth to retrieve the velocities observed (see supplementary figures 5 and 7).

However, such a rigid block model and elastic approach has some limitations. First, the east-

ern boundary of the Andean sliver is not well defined south of 26°S since no clear dominant active front has been detected in the Sierras Pampeanas and South of them. The deformation in the Sierras Pampeanas is diffuse and taken by several active structures and therefore can not be retrieved using an elastic block model approach. As a result, our best-model fails to retrieve the details of the deformation in this region. Second, it is well known now that a large part of the interseismic deformation observed in the middle to far field of rapid subduction zones can be explained by visco-elastic loading models as it has been proposed for North Chile (LI et al., 2015), Sumatra and Japan (TRUBIENKO et al., 2013). However, it is to note that the deformations predicted in the near field by both elastic and visco-elastic approach are similar (TRUBIENKO et al., 2013). Therefore, we are confident that our simple elastic model retrieves well the first order pattern of deformation in the near field of the subduction fault and in particular the small-scale along-strike variations of the coupling coefficient, but the sliver motion, the residual velocities observed in mid and far field (see supplementary figure 4), and the coupling distribution with depth have to be interpreted with extreme caution.

Despite these limitations and keeping them in mind, it is interesting to note that the Euler pole found for the Andean Sliver implies a decreasing backarc shortening rate from North to South Chile and an overall clockwise rotation of the entire sliver. These broad characteristics of the deformation are in agreement with several paleomagnetic studies that have been conducted in the last decades (e.g ARRIAGADA et al., 2008), and suggest that the deformation averaged in the region since Paleogene may still be going on today. An other argument in favor of a persistent motion of the Andean block on long time-scale is the fact that residuals pointing North are observed in the mid-field in Central Chile (supplementary figure 4) suggesting that the North-

Eastward block motion imposed by our inversion does not account for part of the deformation in the North-South direction in this region. This northward motion in the Central Chile principal cordillera has been also described in the cumulated deformation pattern observed over several million years ARRIAGADA et al. (2008).

5.2 The Chilean margin is segmented

The small-scale along-strike variations of the amount of coupling are preserved whatever the smoothing coefficient and shortening amount taken by the sliver motion, and therefore considered robust (Fig.3-B and supplementary figure 5). The along-dip variations of the coupling coefficient are less well constrained since they mainly impact the vertical deformation pattern that is poorly known compared to the horizontal deformation (see supplementary figure 1). Insar images offering dense measurements of the upper plate deformation dominated by the vertical signal, together with continuous GPS data could help constraining better the downdip extent of the highly coupled zone (e.g BÉJAR-PIZARRO et al., 2009; DUCRET et al., 2012). Overall, the highly coupled zones ($\Phi > 80\%$) do not extend bellow 60 km depth. Whether these nearly locked patches spread up to the trench is beyond the resolution of our model (see section 4).

We define the average coupling at a given position along the trench as the integration of the coupling coefficient over depth, from surface to 60 km depth, i.e.the supposed downdip limit of the seismogenic zone. The profile of the average coupling versus latitude shown in Figure 3B images a succession of 7 large highly coupled segments bounded by 6 narrow low coupled zones (LCZ). We define these LCZs as areas of abrupt decrease in the average coupling surrounded

by zones where coupling is higher and relatively stable. Since a single threshold value valid for the entire trench could not be identified, the definition of a LCZ is local. Some LCZs are associated with a clear interruption of the highly locked zone in map view (Baranquilla, Iquique, see Fig.3C) while the locked zone only narrows in others (La Serena, San Antonio, Mejillones). In addition to the six clearest LCZs, three other areas exhibit a slight decrease in average coupling : in front of Constitución ($\sim$35°S, already identified by MORENO et al. (2010)), another in front of Los Vilos ($\sim$32°S), and finally offshore Arica ($\sim$18°S). These features have not been always detected in previous works and appear more model-dependent than the others (in particular, they are barely visible in the 2-plate models, see supplementary figure 7). This is probably due to the fact that they are characterized by a decrease in the coupling on the 30 to 60 km depth part of the interface, i.e. they are associated with a sharpening of the transition zone from the deep creeping portion to the shallow zone that remains highly coupled. Opposite, in most of the other LCZs, coupling decreases even in the shallowest part of the fault. The Los Vilos LCZs ($\sim$32°S) also correlates with an abrupt change in the slab geometry that flattens at 100 km depth and an important increase in the background seismicity rate (Fig.2).

The comparison between the average coupling calculated for 2-plate and 3-plate models (supplementary figure 5) shows that the segmentation of the margin (small-scale along-strike variations) is preserved while the average coupling tends to decrease significantly North of 24°S in the 3-plate models. This may be due to the fact that the Andean block motion in this area decreases the effective convergence rate on the subduction interface by 1 cm/yr, or to the fact that the coupling values are lower in the shallowest unresolved part of the interface in the 3-plate models than in the 2-plate models. Thus, we interpret this large-scale decrease of the average coupling

as an artifact coming from our modeling strategy rather than a true feature that would correlate with changes in the subduction style for instance.

The recent establishment of interseismic coupling maps along several subduction zones has enlightened that along-strike and along-dip variations of the coupling coefficient are common features that may come from general characteristics of these plate boundaries. For instance, WANG and BILEK (2014) claim that LCZs correlate with the subduction of major bathymetric features of the subducted plate, while BÉJAR-PIZARRO et al. (2013) relate coupling coefficient to geological and tectonic complexities of the upper plate. In Chile, 5 of the 6 well-identified LCZs correlate with the subduction of ridges or fracture zones of the Nazca plate (high oceanic features, or HOFs) that enters into subduction (Iquique, Baranquilla, La Serena, San Antonio and Arauco LCZs), and all of them are associated to singularities in the coast-line morphology (peninsulas, bays) often related to crustal fault networks. Whatever the hypothesis considered, the correlation between coupling calculated from interseismic velocities acquired on few years of measurement and long-term geological and morphological features is a strong argument in favor of a relative stability in time and space of the interseismic coupling segmentation. Mechanical models considering the interaction between both plates during several seismic cycles should help in the future to tackle this issue. In any case, in Chile, most of the HOFs that are thought to control the coupling coefficient are oblique relative to the convergence velocity between both plates and should therefore be migrating significantly along the trench even at the time scale of several seismic cycles, challenging the hypothesis of a long-term structural control of coupling by HOFs.

In the following we do not concentrate on the factors controlling the variations of the coupling

coefficient but rather focus on the interpretation of the coupling maps in terms of mechanical behaviour of the interface.

5.3 Segmentation and megathrusts

Rupture zones of historical megathrust earthquakes documented in Chile since the 18th century (e.g LOMNITZ, 1970; COMTE and PARDO, 1991) often correlate with highly coupled segments, suggesting that the zones where apparent interseismic coupling is high are regions of velocity-weakening behaviour (Fig.2). On the other hand, LCZs are seldom crossed by megathrust ruptures and often behave as barriers to their propagation (KANEKO et al., 2010) : more than 60% of the historical major ruptures in Chile are stopped or initiated near LCZs while no more than 15% propagated through them.

Only giant earthquakes seem to make their way trough some very low-coupling regions like the 1730 or 1922 Mw$\sim$9 events. These zones where the average coupling can reach values as low as 40% could therefore be associated with areas of velocity-strengthening behaviour, i.e. able to slow down or stop rupture propagation. This correlation between coupling and mechanical behaviour should be carefully considered because of the stress-shadow effect produced by locked velocity-weakening areas in their vicinity that may lead to apparent high coupling in velocity-strengthening zones (e.g BÜRGMANN et al., 2005; HETLAND and SIMONS, 2010; MÉTOIS et al., 2012). In other words : a small LCZ may be invisible in the upper plate deformation pattern, if bounded by sufficiently large locked asperities.

The recent Maule (2010, Mw 8.8), Iquique (2014, Mw 8.1) and Illapel (2015, Mw 8.4) events

allow for a detailed comparison of interseismic coupling with coseismic slip distributions. We plot in Fig.3B both the average coupling and the average coseismic slip for each of these events, and in Fig.4 their associated coseismic distribution by (VIGNY et al., 2011; LAY et al., 2014; RUIZ et al., 2016). As already shown by several authors for the Maule and Iquique earthquakes (MORENO et al., 2010; MÉTOIS et al., 2012; RUIZ et al., 2014; SCHURR et al., 2014), the first-order correlation between highly coupled segment and megathrust rupture is confirmed. In particular, all of these mega-earthquakes ruptures stopped when entering into a LCZ. In Figure 5, we plot the coseismic slip versus the prevailing interseismic coupling Φ for each subfaults located in the megathrust ruptures zones and we calculate the conditional probability $P_{>1.5m/\Phi}$ of experiencing more than 1.5 meter of coseismic slip depending on the value of prevailing interseismic coupling Φ defined as :

$$P_{>1.5m/\Phi} = \frac{N_{subfaults_{>1.5m/\Phi}}}{N_{subfaults_{\Phi}}}$$

These plots show that for all of three earthquakes, high coseismic slip is only observed in highly coupled subfaults, and that the correlation between the probability of experiencing more than 1.5 meter of coseismic slip and the coupling Φ is $\sim 90\%$ for the Maule and Illapel earthquakes. The Iquique case appears more complex since the coefficient of correlation is only 56%. We interpret this lower correlation between prevailing interseismic coupling and the coseismic slip distribution for the Iquique earthquake as the result of the combined lack of resolution in the offshore part of the subduction interface for both coseismic and interseismic coupling models due to the large distance between the coast and the trench ($\sim$150 km). One other possible cause

for the absence of striking correlation in the Iquique case is the fact that this event is relatively small compared to the Illapel and Maule events (Mw 8.1), and occurred in a swarm and slow slip context (e.g. RUIZ et al., 2014; SCHURR et al., 2014). It could be that the prevailing slow-slip event has released part of the slip that should have been released coseismically in a more standard megathrust rupture scenario, therefore biasing the correlation between interseismic coupling and coseismic slip.

Overall, in the case of the 2014 Iquique event, the earthquake ruptured the "Camarones" highly-coupled segment (in a region where the model resolution is lowest than elsewhere) and has been stopped southward by the Iquique LCZ (RUIZ et al., 2014; SCHURR et al., 2014). The recent Illapel earthquake nucleated near a small LCZ at 32°S, ruptured the highly coupled patch forming the northern part of the Metropolitan segment in between the subduction points of the Challenger fracture zone and of the Juan Fernandez ridge, and stopped northward at 30°S in the large La Serena LCZ (YE et al., 2015; RUIZ et al., 2016).

The Mw 8.8 Maule earthquake has a complex bi-lateral propagation that may reflect heterogeneities in the pre-existing coupling or in the interface properties (MORENO et al., 2010; MÉTOIS et al., 2012) but also stopped at two LCZs : San Antonio in the North and Arauco in the South. An interesting feature of this earthquake is the very large coseismic slip observed in front of Constitución (35.2°S) where the average coupling calculated on the first 60 km depth is relatively low. This apparent contradiction has been interpreted by several authors as an evidence for dynamic propagation of the rupture through a previously creeping zone (MORENO et al., 2010), while other interseismic models were evidencing only a small decrease in the coupling coefficient at this latitude (MÉTOIS et al., 2012). However, as explained in section 5.2, the

highly coupled zone does not interupt in the Constitución LCZ but is rather associated with a very sharp transition zone. To our opinion, this sharpening of the transition zone is consistent with an increase in coseismic slip in the upper portion of the interface. A possible scenario could be that the rupture coming from the South would have been unabled to propagate in the 30 to 60 km deep portion of the interface since the transition zone was too sharp, thus increasing the stress on the highly coupled upper part of the fault, leading to a higher shallow coseismic slip.

Last but not least, the remaining unbroken portion of the Metropolitan segment is highly coupled (in fact was highly coupled before the Maule rupture) and should be considered with extreme caution : indeed there, stress has been increased by the neighbouring ruptures but is simultaneously slowly released by viscous relaxation (KLEIN et al., 2016). However, this release rate is small compared to the long-term accumulation and the remaining high coupling zone could probably still rupture with a Mw>8 event. Further detailed slip-budgets are difficult to conduct on the Chilean subduction zone because (i) the spatial resolution of all coseismic slip and interseismic slip models is limited, in particular in the shallowest part of the interface; (ii) we lack insights on the slip distribution of the historical coseismic ruptures (namely the 1835, 1877 and 1922 earthquakes preceeding the Maule, Iquique and Illapel earthquakes, respectively); and (iii) we do not know today the portion of the plate convergence that could be accommodated by slow-slip events on the subduction interface. In any case, based on the Chilean example, knowing the interseismic coupling allows for a rather good estimate of the size and shape of the coming ruptures, while the timing of such ruptures remains poorly understood.

5.4 Interseismic coupling and background seismicity

All three Mw>8 megathrust earthquakes that stroke Chile in the last years were preceded by large intraplate events rupturing the oceanic slab between 60 and 120 km depth several years of decades before (Fig.4). The Tarapacá Mw 7.8 earthquake ruptured in 2005 onshore of Iquique, the Chillán Mw 8.3 event devastated the Maule region in 1939 and the Punitaqui Mw 7.1 event was strongly felt in the Illapel area in 1997. The only other significant intraslab earthquake that has been reported over the margin is the deep 1950 Calama event that was followed by the shallower Antofagasta Mw 8 megathrust earthquake in 1995 (Fig.2). This succession of large intraplate and large megathrust earthquakes raises the issue of a possible indirect triggering of megathrust ruptures (over tens of years) by changes in stress on the deep part of the subduction interface as suggested by KAUSEL and CAMPOS (1992) and BIE and RYDER (2015), or by a more complex triggering mechanism through a slow spread of deformation as observed in Greece (DURAND et al., 2014). More generally, it raises the question of the link between intraslab earthquakes, the background seismicity, the coupling and the megathrust rupture.

The first-order mechanical interpretation of interseismic coupling in the rate-and-state formalism implies that during interseismic loading, the LCZs should creep while the coupled segments should remain stuck. Therefore, aseismic transients should be registered near the LCZ. However, opposite to most of the world's subduction zones, no slow-slip event (SSE) has been observed along the Chilean subduction zone before the potential SSE that preceded the 2014 Mw 8.2 Iquique earthquake (RUIZ et al., 2014; SCHURR et al., 2014; LAY et al., 2014; KATO and NAKAGAWA, 2014).

In order to better understand the mechanical behaviour of the LCZs and segments, we analyzed the background seismic activity (3 <Mw<7 earthquakes) during the interseismic phase between two megathrust earthquakes based on the CSN catalogue (*http://www.sismologia.cl/*, complete for Mw>3 since 2000). We consider different periods representative of the interseismic background seismicity along the margin : from 2000 to 2010 for South-Central Chile (before the Maule event), from 2008 to 2014 for North Chile (between the Tarapaca and Iquique events), and from 2000 to 2014 for Central Chile (see Fig.2). On Figure 3-A, where we plot the along-strike evolution of the seismicity rate together with the swarms that have been detected in Chile (HOLTKAMP et al., 2011; RUIZ et al., 2014), three seismic gaps, i.e. zones that experience very few moderate magnitude earthquakes, are clearly identified : the Maule, Loa and Paranal-Chanaral area that also correspond to highly coupled segments. There, no or few earthquakes occur where coupling is higher than 80% (Fig.4). In contrast, the Camarones segment was relatively active during the interseismic period even in the 80% coupled zones, but seismicity and swarms (among which the preseismic sequence before the Iquique main shock see Fig.4) mainly concentrate on the edges of the high coupling zone, near the Iquique LCZ. Finally, the Metropolitan segment is the most active portion of the Chilean subduction zone during the interseismic phase (Figs.2 and 4) with more than 50 Mw>3 events per year on its edges, and at least 20 events per year in the highly coupled portion of the segment. The strong increase in seismicity rate between the Maule and Metropolitan segments appears correlated with the flattening of the deep portion of the slab.

Overall, it seems that higher seismicity rates are observed in or near the LCZs, while segments tend to be more silent during interseismic phase. However, the Metropolitan region be-

haves completely differently of this simple scheme since both seismicity and coupling are high. This first order analysis conducted with the CSN catalog suffers obviously from the heterogeneity in the epicenters location accuracy, and from the completeness threshold of the catalog. More detailed and regional analysis are required to really conclude on the spatial relationship between moderate magnitude earthquakes and coupling.

However, interestingly, several swarm-like sequences occurring along the Chilean subduction zone have been recently pointed out by declustering methods applied to the CSN catalog (HOLTKAMP et al., 2011; RUIZ et al., 2014). 8 of these 10 non-volcanic swarm sequences happen to be located at the transition zone between segments and LCZ (Figs.2A and 4), in agreement with recent observations along other subduction zones (HOLTKAMP and BRUDZINSKI, 2014). Little is known today about the kinematics and dynamics of theses clusters that would require systematic relocation and analysis, but they emphasize a specific mechanical behaviour of the subduction interface between segments and LCZs. It is to note that several of the shallowest swarms have been attributed to HOFs located in the shallow portion of the fault (e.g. COMTE et al., 2002; THIERER et al., 2005; CONTRERAS-REYES and CARRIZO, 2011). For instance, the shallow seismic sequences located offshore San Antonio and Valparaiso are thought to be associated with deformation of the fore-arc enhanced by the subduction of fractured seamounts forming the Juan Fernandez ridge complex (THIERER et al., 2005). This is in agreement with the good correlation observed between the LCZs and the inception of HOFs (see section 5.2) and suggests a link between the subducting plate structure, the mechanical behaviour of the interface and the geodetic coupling coefficient. However, how HOFs may influence the mechanical behaviour of the subduction fault remains unclear : the fracturation of the downgoing plate may

directly favor fluid migration and modify the fluid pressure on the interface, but HOFs could also behave as barriers to sediment filling of the trench and modify the structure of the sedimentary prism directly involved in the faulting processes. In Chile, the latter effect is confirmed by the correlation observed between HOFs and positive gravity anomalies (e.g. SONG and SIMONS, 2003; SOBIESIAK et al., 2007; ÁLVAREZ et al., 2014; MAKSYMOWICZ, 2015). A relationship may exist between the interseismic coupling coefficient, the friction coefficient on the fault and the structure of the sedimentary prism as proposed for the Guerrero subduction zone by ROUSSET et al. (2015) or in the Maule area (CUBAS et al., 2013), but remains to be tested.

5.5 Creeping low-coupled zones ?

Since these swarms generally occur at the edges of LCZs, they could be an indirect sign that slow slip events (SSE) occur in the center of the LCZ and would reveal the existence of small-scale velocity-weakening patches located preferentially at the transition zone toward velocity-weakening dominant segments. This interpretation is consistent with observations made on several subduction zones where SSEs have been observed together with swarm seismicity (e.g. ROGERS and DRAGERT, 2003; VALLEE et al., 2013); and with recent numerical models (e.g HETLAND and SIMONS, 2010; KANEKO et al., 2010).

However, no short-term SSE had been registered in these swarm-prone areas or elsewhere in Chile before the recent 2014 Iquique precursory sequence (RUIZ et al., 2014). This could be due to an observation bias since continuous GPS stations are operating in Chile only since 1995 for the oldest, and since 2004 for most of them, and that they are not homogeneously distributed over

the Chilean coast. Indeed, most of the swarm sequences reported by HOLTKAMP et al. (2011) occurred before 1990, and only one cGPS station located far from the trench was operative during the 2006 Baranquilla swarm (Copiapó station, 27°S) showing no clear evidence for transient motion (COMTE et al., 2002; HOLTKAMP et al., 2011). The swarms that occurred since 2008 offshore Iquique (Fig.4) were located in the less resolved part of the subduction zone, i.e. where the distance between the coast, the cGPS stations and the trench is the highest, preventing for clear detection of associated SSE.

Nevertheless, since the widest well resolved La Serena and Iquique LCZs are instrumented by dense cGPS networks since $\sim$2004, we infer that no small-duration transient slip comparable to the Mexican or Cascadian SSEs that usually produce centimeters of displacements on c-GPS time-series has occurred there since 10 years (e.g VERGNOLLE et al., 2010). If a Mw 6.5 SSE would occur in the very shallow part of the slab in the best-resolved part of our model, i.e. in front of the Tongoy Peninsula (30°S), it would produce a $\sim$0.5 cm offset on the East component of the closest continuous GPS station and less than a millimeter displacement on North and Vertical components (see supplementary figure 9). If spread over several months, such an event would probably remain hidden under the seasonnal variations and remain undetected in the continuous time-series. Therefore, if creeping occurred in the La Serena LCZ, it must have been either very slow slip events (VSSE, RUIZ et al., 2014) occurring on tens of years, or short-term SSE that would remain beyond the detectability threshold of our network, i.e. on the shallowest part of the slab.

If all the swarm events detected in Chile by HOLTKAMP et al. (2011) are located at the segment-LCZ transition zones, not all LCZs have experienced swarms (Mejillones, Constitu-

ción, see Fig.3). This lack of swarm activity during the interseismic period could be interpreted as an evidence for a smooth fault interface that could be creeping silently (HOLTKAMP and BRUDZINSKI, 2014), while the number and intensity of swarms in the other LCZs may reflect the density of small-scale velocity-weakening asperities. It is also possible that in some cases, the activity of LCZs is controlled by the roughness of the subducted oceanic plate while in others, coupling is decreased by the connection between crustal fault networks and the subduction interface and not by a change in interface roughness. This could be the case for the Mejillones Peninsula LCZ where large crustal fault networks have been imaged and could reach the subduction interface inducing a lower coupling coefficient without swarm activity. However, we have probably missed some swarm sequences in the CSN catalog or the catalog is too short to get a representative swarm distribution, and therefore we can not rule out the fact that swarms will occur in the vicinity of the Mejillones LCZ.

6 Conclusions

We derived an almost continuous distribution of interseismic coupling along the Chilean coast (18-38°S) that reproduces reasonably well the GPS measurements conducted along the margin since the early 90's. These data are overall consistent with highly variable coupling on the subduction zone and a clockwise rotation motion of the Andean sliver that produces 1 cm/yr eastward motion in the Bolivian Andes and few mm/yr at the Maule region latitudes ($\sim$38°S).

The comparison between the interseismic coupling and the three large megathrust ruptures that stroke Chile in the last 5 years confirms a very good correlation between high coseismic slip

and high coupling, while ruptures stopped in LCZ. Therefore, coupling coefficient could be used as a good proxy to assess the location and shape of future megathrust ruptures, even if we still lack understanding on the timing of these ruptures and on their overall magnitude.

Detailed analysis of the background seismicity registered by the Chilean catalogue (CSN) demonstrates that often, no simple relationship exists between the moderate seismicity and the coupling coefficient. The three Chilean seismic gaps exhibit very low rates of background seismicity that concentrate in intermediate to low coupling areas suggesting that highly coupled zones correspond to fully locked velocity-weakening asperities, but this relationship vanished in the Metropolitan or the Camarones segments.

Seismic swarms occur in general at the transition between highly coupled segments and low-coupled zones (LCZs), suggesting that LCZs behave as velocity-strengthening material sliding aseismically and triggering swarms on their vicinity. Even if no short-term SSE have been detected there in the last decade in Chile, LCZs and notably the La Serena area are probably experiencing either shallow undetected SSE or very long-term SSE ranging on several decades. Since most of these LCZs behaved as barriers to the propagation of past and recent megathrust earthquakes and could be involved in their nucleation process as it has been the case for the 2014 Mw 8.2 Iquique earthquake, they should be the focus of special attention by the community in the future.

Acknowledgments

We are grateful to all people that have been involved throughout the years in the field work and maintenance of the GPS network, in particular D.Carrizo, A.Delorme, S.Peyrat, C.Bermejo and I.Ortega. This work has been supported by LiA “Montessus de Ballore” and received partial support from grants ANR-2011-BS56-017 and ANR-2012-BS06-004 of the French "Agence Nationale de la Recherche (ANR). GPS receivers for campaign measurements were provided by RESIF (Réseau sismologique français). We thank Rob McCaffrey for freely providing Tdefnode, and the Centro Sismologico Nacional of Universidad de Chile, Santiago, for making their catalog available. All the figures have been done using Generic Mapping Tools. We thank two anonymous reviewers for their useful comments on this work.

References

ÁLVAREZ, O., NACIF, S., GIMENEZ, M., FOLGUERA, A., and BRAITENBERG, C. (2014). Goce derived vertical gravity gradient delineates great earthquake rupture zones along the chilean margin. *Tectonophysics*,doi:10.1016/j.tecto.2014.03.011, 622:198–215.

ARÁNGUIZ, R., GONZÁLEZ, G., GONZÁLEZ, J., CATALÁN, P.A, CIENFUEGOS, R., YAGI, Y., OKUWAKI, R., URRA, L., CONTRERAS, K., DEL RIO, I. ET AL. (2016) The 16 September 2015 Chile Tsunami from the Post-Tsunami Survey and Numerical Modeling Perspectives *Pure and Applied Geophysics*,1–16.

ARGUS, D. F., GORDON, R. G., and DEMETS, C. (2011). Geologically current motion of 56

554 plates relative to the no-net-rotation reference frame. *Geochemistry, Geophysics, Geosystems*,
555 doi: 10.1029/2011GC003751, 12(11).

556 ARMIJO, R., RAULD, R., THIELE, R., VARGAS, G., CAMPOS, J., LACASSIN, R., and
557 KAUSEL, E. (2010). The west andean thrust, the san ramón fault, and the seismic hazard
558 for santiago, chile. *Tectonics*, doi: 10.1029/2008TC002427, 29(2).

559 ARMIJO, R. and THIELE, R. (1990). Active faulting in northern Chile: ramp stacking and
560 lateral decoupling along a subduction plate boundary? *Earth and Planetary Science Letters*,
561 doi:10.1016/0012-821X(90)90087-E, 98(1):40–61.

562 ARRIAGADA, C., ROPERCH, P., MPODOZIS, C., and COBBOLD, P. (2008). Paleogene build-
563 ing of the bolivian orocline: Tectonic restoration of the central andes in 2-d map view. *Tecton-*
564 *ics*, doi: 10.1029/2008TC002269, 27(6).

565 BÉJAR-PIZARRO, M., CARRIZO, D., SOCQUET, A., ARMIJO, R., BARRIENTOS, S., BON-
566 DOUX, F., BONVALOT, S., CAMPOS, J., COMTE, D., DE CHABALIER, J., ET AL. (2009).
567 Asperities and barriers on the seismogenic zone in North Chile: state-of-the-art after the 2007
568 Mw 7.7 Tocopilla earthquake inferred by GPS and InSAR data. *Geophysical Journal Interna-*
569 *tional*, doi: 10.1111/j.1365-246X.2010.04748.x.

570 BÉJAR-PIZARRO, M., SOCQUET, A., ARMIJO, R., CARRIZO, D., GENRICH, J., and SIMONS,
571 M. (2013). Andean structural control on interseismic coupling in the north chile subduction
572 zone. *Nature Geoscience*, doi:10.1038/ngeo1802, 6(6):462–467.

573 BEVIS, M., KENDRICK, E., SMALLEY JR, R., BROOKS, B., ALLMENDINGER, R., and

ISACKS, B. (2001). On the strength of interplate coupling and the rate of back arc convergence in the central Andes: An analysis of the interseismic velocity field. *Geochemistry Geophysics Geosystems*, doi: 10.1029/2001GC000198, 2(11):1067.

BEVIS, M., KENDRICK, E., SMALLEY JR, R., HERRING, T., GODOY, J., and GALBAN, F. (1999). Crustal motion north and south of the Arica deflection: comparing recent geodetic results from the Central Andes. *Geochemistry Geophysics Geosystems*, doi: 10.1029/1999GC000011, 1(12):1005.

BIE, L. and RYDER, I. (2015). The 2005 tarapaca earthquake: a likely indirect trigger of the 2014 iquique earthquake. In *EGU General Assembly Conference Abstracts*, volume 17, page 10013.

BROOKS, B., BEVIS, M., SMALLEY JR, R., KENDRICK, E., MANCEDA, R., LAURÍA, E., MATURANA, R., and ARAUJO, M. (2003). Crustal motion in the Southern Andes (26–36 S): Do the Andes behave like a microplate? *Geochemistry Geophysics Geosystems*, doi: 10.1029/2003GC000505, 4(10):1085.

BROOKS, B., BEVIS, M., WHIPPLE, K., ARROWSMITH, J., FOSTER, J., ZAPATA, T., KENDRICK, E., MINAYA, E., ECHALAR, A., BLANCO, M., ET AL. (2011). Orogenic-wedge deformation and potential for great earthquakes in the central andean backarc. *Nature Geoscience*, doi:10.1038/ngeo1143, 4(6):380–383.

BÜRGMANN, R., KOGAN, M. G., STEBLOV, G. M., HILLEY, G., LEVIN, V. E., and APEL, E. (2005). Interseismic coupling and asperity distribution along the kamchatka subduction zone. *Journal of Geophysical Research: Solid Earth*, doi: 10.1029/2005JB003648, 110(B7).

595 CALISTO, I., MILLER, M., and CONSTANZO, I. (2016). Comparison between tsunami signals
596 generated by different source models and the observed data of the illapel 2015 earthquake.
597 *Pure and Applied Geophysics*, pages 1–11.

598 CHLIEH, M., AVOUAC, J., SIEH, K., NATAWIDJAJA, D. H., and GALETZKA, J. (2008).
599 Heterogeneous coupling of the sumatran megathrust constrained by geodetic and paleo-
600 geodetic measurements. *Journal of Geophysical Research: Solid Earth (1978–2012)*, doi:
601 10.1029/2007JB004981 113(B5).

602 CHLIEH, M., PERFETTINI, H., TAVERA, H., AVOUAC, J., REMY, D., NOCQUET, J., ROLAN-
603 DONE, F., BONDOUX, F., GABALDA, G., and BONVALOT, S. (2011). Interseismic coupling
604 and seismic potential along the central andes subduction zone. *Journal of Geophysical Re-*
605 *search*, doi: 10.1029/2010JB008166, 116(B12):B12405.

606 COMTE, D., HAESSLER, H., DORBATH, L., PARDO, M., MONFRET, T., LAVENU, A., PON-
607 TOISE, B., and HELLO, Y. (2002). Seismicity and stress distribution in the copiapo, northern
608 chile subduction zone using combined on-and off-shore seismic observations. *Physics of the*
609 *earth and planetary interiors*, doi:10.1016/S0031-9201(02)00052-3, 132(1):197–217.

610 COMTE, D. and PARDO, M. (1991). Reappraisal of great historical earthquakes in the northern
611 Chile and southern Peru seismic gaps. *Natural Hazards*, 4(1):23–44.

612 CONTRERAS-REYES, E. and CARRIZO, D. (2011). Control of high oceanic features and sub-
613 duction channel on earthquake ruptures along the chile–peru subduction zone. *Physics of the*
614 *Earth and Planetary Interiors*, doi:10.1016/j.pepi.2011.03.002, 186(1):49–58.

615 CUBAS, N., AVOUAC, J., SOULOUMIAC, P., and LEROY, Y. (2013). Megathrust friction de-
616 termined from mechanical analysis of the forearc in the maule earthquake area. *Earth and*
617 *Planetary Science Letters*, doi:10.1016/j.epsl.2013.07.037, 381:92–103.

618 DEMETS, C., GORDON, R. G., ARGUS, D. F., and STEIN, S. (1994). Effect of recent revisions
619 to the geomagnetic reversal time scale on estimates of current plate motions. *Geophysical*
620 *research letters*, doi: 10.1029/94GL02118, 21(20):2191–2194.

621 DUCRET, G., DOIN, M., GRANDIN, R., SOCQUET, A., VIGNY, C., MÉTOIS, M., and BÉJAR-
622 PIZZARO, M. (2012). Measurement of interseismic strain accumulation in the southern andes
623 (25°-35° s) using envisat sar data. In *EGU General Assembly Conference Abstracts*, vol-
624 ume 14, page 10391.

625 DURAND, V., BOUCHON, M., FLOYD, M. A., THEODULIDIS, N., MARSAN, D., KARAB-
626 ULUT, H., and SCHMITTBUHL, J. (2014). Observation of the spread of slow defor-
627 mation in greece following the breakup of the slab. *Geophysical Research Letters*, doi:
628 10.1002/2014GL061408, 41(20):7129–7134.

629 GARDNER, J. and KNOPOFF, L. (1974). Is the sequence of earthquakes in southern california,
630 with aftershocks removed, poissonian. *Bull. Seismol. Soc. Am*, 64(5):1363–1367.

631 HAYES, G. P., WALD, D. J., and JOHNSON, R. L. (2012). Slab1. 0: A three-dimensional
632 model of global subduction zone geometries. *Journal of Geophysical Research: Solid Earth*
633 *(1978–2012)*, doi: 10.1029/2011JB008524 117(B1).

634 HETLAND, E. and SIMONS, M. (2010). Post-seismic and interseismic fault creep II: transient

creep and interseismic stress shadows on megathrusts. *Geophysical Journal International*, doi: 10.1111/j.1365-246X.2009.04482.x, 181(1):99–112.

HOFFMANN-ROTHE, A., KUKOWSKI, N., DRESEN, G., ECHTLER, H., ONCKEN, O., KLOTZ, J., SCHEUBER, E., and KELLNER, A. (2006). Oblique convergence along the Chilean margin: partitioning, margin-parallel faulting and force interaction at the plate interface. *The Andes*, pages 125–146.

HOLTKAMP, S. and BRUDZINSKI, M. R. (2014). Megathrust earthquake swarms indicate frictional changes which delimit large earthquake ruptures. *Earth and Planetary Science Letters*, doi:10.1016/j.epsl.2013.10.033, 390:234–243.

HOLTKAMP, S. G., PRITCHARD, M., and LOHMAN, R. (2011). Earthquake swarms in South America. *Geophysical Journal International*, doi: 10.1111/j.1365-246X.2011.05137.x, 187(1):128–146.

KANEKO, Y., AVOUAC, J., and LAPUSTA, N. (2010). Towards inferring earthquake patterns from geodetic observations of interseismic coupling. *Nature Geoscience*, doi:10.1038/ngeo843, 3(5):363–369.

KATO, A. and NAKAGAWA, S. (2014). Multiple slow-slip events during a foreshock sequence of the 2014 iquique, chile Mw 8.1 earthquake. *Geophysical Research Letters*, doi: 10.1002/2014GL061138, 41(15):5420–5427.

KATO, A., OBARA, K., IGARASHI, T., TSURUOKA, H., NAKAGAWA, S., and HIRATA, N. (2012). Propagation of slow slip leading up to the 2011 mw 9.0 tohoku-oki earthquake.

655 *Science*, doi: 10.1126/science.1215141, 335(6069):705–708.

656 KAUSEL, E. and CAMPOS, J. (1992). The Ms= 8 tensional earthquake of 9 december 1950 of
657 northern chile and its relation to the seismic potential of the region. *Physics of the earth and*
658 *planetary interiors*, doi:10.1016/0031-9201(92)90203-8, 72(3):220–235.

659 KENDRICK, E., BEVIS, M., SMALLEY, R., and BROOKS, B. (2001). An integrated crustal ve-
660 locity field for the central Andes. *Geochem. Geophys. Geosyst*, doi: 10.1029/2001GC000191,
661 2(11):1066.

662 KHAZARADZE, G. and KLOTZ, J. (2003). Short-and long-term effects of GPS measured
663 crustal deformation rates along the south central Andes. *Journal of geophysical research*,
664 doi: 10.1029/2002JB001879, 108(B6):2289.

665 KLEIN, E., FLEITOUT, L., VIGNY, C., and GARAUD, J. (2016). Afterslip and viscoelastic
666 relaxation model inferred from the large scale postseismic deformation following the 2010 Mw
667 8,8 Maule earthquake (Chile). *Accepted for publication in Geophysical Journal International*.

668 KLOTZ, J., KHAZARADZE, G., ANGERMANN, D., REIGBER, C., PERDOMO, R., and CI-
669 FUENTES, O. (2001). Earthquake cycle dominates contemporary crustal deformation in
670 Central and Southern Andes. *Earth and Planetary Science Letters*, doi:10.1016/S0012-
671 821X(01)00532-5, 193(3-4):437–446.

672 KONCA, A., AVOUAC, J., SLADEN, A., MELTZNER, A., SIEH, K., FANG, P., LI, Z., GALET-
673 ZKA, J., GENRICH, J., CHLIEH, M., ET AL. (2008). Partial rupture of a locked patch of the
674 Sumatra megathrust during the 2007 earthquake sequence. *Nature*, doi:10.1038/nature07572,

456(7222):631–635.

LAY, T., YUE, H., BRODSKY, E. E., and AN, C. (2014). The 1 April 2014 Iquique, Chile, Mw 8.1 earthquake rupture sequence. *Geophysical Research Letters*, doi: 10.1002/2014GL060238, 41(11):3818–3825.

LI, S., MORENO, M., BEDFORD, J., ROSENAU, M., and ONCKEN, O. (2015). Revisiting visco-elastic effects on interseismic deformation and locking degree: a case study of the Peru-North Chile subduction zone. *Journal of Geophysical Research: Solid Earth*, doi: 10.1002/2015JB011903.

LOMNITZ, C. (1970). Major earthquakes and tsunamis in Chile during the period 1535 to 1955. *International Journal of Earth Sciences*, 59(3):938–960.

LOVELESS, J. and MEADE, B. (2011). Spatial correlation of interseismic coupling and coseismic rupture extent of the 2011 Mw9.0 Tohoku-Oki earthquake. *Geophys. Res. Lett*, doi: 10.1029/2011GL048561, 38:L17306.

MAKSYMOWICZ, A. (2015). The geometry of the Chilean continental wedge: Tectonic segmentation of subduction processes off Chile. *Tectonophysics*, doi:10.1016/j.tecto.2015.08.007, 659:183–196.

MAROT, M., MONFRET, T., GERBAULT, M., NOLET, G., RANALLI, G., and PARDO, M. (2014). Flat versus normal subduction zones: a comparison based on 3-d regional traveltime tomography and petrological modelling of central chile and western Argentina (29°–35°s). *Geophysical Journal International*, doi: 10.1093/gji/ggu355, 199(3):1633–1654.

695 McCaffrey, R. (2002). Crustal block rotations and plate coupling. *Plate Boundary Zones,*
696 *Geodyn. Ser*, doi: 10.1029/GD030p0101, 30:101–122.

697 McCaffrey, R. (2009). Time-dependent inversion of three-component continuous gps for
698 steady and transient sources in northern Cascadia. *Geophysical Research Letters*, doi:
699 10.1029/2008GL036784, 36(7).

700 McCaffrey, R. (2014). Interseismic locking on the Hikurangi subduction zone: Un-
701 certainties from slow-slip events. *Journal of Geophysical Research: Solid Earth*, doi:
702 10.1002/2014JB010945 119(10):7874–7888.

703 Melnick, D. and Bookhagen, B. (2009). Segmentation of megathrust rupture zones from
704 fore-arc deformation patterns over hundreds to millions of years, Arauco peninsula, Chile.
705 *Journal of Geophysical Research. B. Solid Earth*, doi: 10.1029/2008JB005788, 114.

706 Métois, M., Socquet, A., and Vigny, C. (2012). Interseismic coupling, segmentation and
707 mechanical behavior of the central chile subduction zone. *Journal of Geophysical Research*,
708 doi: 10.1029/2011JB008736, 117(B3).

709 Métois, M., Socquet, A., Vigny, C., Carrizo, D., Peyrat, S., Delorme, A., Mau-
710 reira, E., Valderas-Bermejo, M.-C., and Ortega, I. (2013). Revisiting the north
711 chile seismic gap segmentation using gps-derived interseismic coupling. *Geophysical Journal*
712 *International*, doi: 10.1093/gji/ggt183, 194(3):1283–1294.

713 Métois, M., Vigny, C., Socquet, A., Delorme, A., Morvan, S., Ortega, I., and
714 Valderas-Bermejo, C.-M. (2014). GPS-derived interseismic coupling on the subduction

715 and seismic hazards in the Atacama region, Chile. *Geophysical Journal International*, doi:
716 10.1093/gji/ggt418, 196(2):644–655.

717 MORENO, M., KLOTZ, J., MELNICK, D., ECHTLER, H., and BATAILLE, K. (2008).
718 Active faulting and heterogeneous deformation across a megathrust segment boundary
719 from GPS data, south central Chile (36–39 S). *Geochem. Geophys. Geosyst*, doi:
720 10.1029/2008GC002198, 9:36–39.

721 MORENO, M., ROSENAU, M., and ONKEN, . (2010). 2010 Maule earthquake slip correlates
722 with pre-seismic locking of Andean subduction zone. *Nature*, doi:10.1038/nature09349, 467.

723 MULLER, R., ROEST, W., ROYER, J., GAHAGAN, L., and SCLATER, J. (1997). Dig-
724 ital isochrons of the world's ocean floor. *Journal of Geophysical Research*, doi:
725 10.1029/96JB01781, 102(B2):3211–3214.

726 NOCQUET, J., VILLEGAS-LANZA, J., CHLIEH, M., MOTHES, P., ROLANDONE, F., JARRIN,
727 P., CISNEROS, D., ALVARADO, A., AUDIN, L., BONDOUX, F., ET AL. (2014). Motion of
728 continental slivers and creeping subduction in the northern Andes. *Nature Geoscience*, doi:
729 10.1038/NGEO2099, 7(4):287–291.

730 NORABUENA, E., LEFFLER-GRIFFIN, L., MAO, A., DIXON, T., STEIN, S., SACKS, I.,
731 OCOLA, L., and ELLIS, M. (1998). Space geodetic observations of Nazca-South Amer-
732 ica convergence across the central Andes. *Science*, doi: 10.1126/science.279.5349.358,
733 279(5349):358.

734 OKADA, Y. (1985). Surface deformation due to shear and tensile faults in a half-space. *Bulletin*

of the Seismological Society of America, 75(4):1135–1154.

REILINGER, R. and KADINSKY-CADE, K. (1985). Earthquake deformation cycle in the Andean back arc, western Argentina. *Journal of Geophysical Research*, doi: 10.1029/JB090iB14p12701, 90(B14):12701–12.

ROGERS, G. and DRAGERT, H. (2003). Episodic tremor and slip on the Cascadia subduction zone: The chatter of silent slip. *Science*, doi: 10.1126/science.1084783, 300(5627):1942–1943.

ROUSSET, B., LASSERRE, C., CUBAS, N., GRAHAM, S., RADIGUET, M., DEMETS, C., SOCQUET, A., CAMPILLO, M., KOSTOGLODOV, V., CABRAL-CANO, E., ET AL. (2015). Lateral variations of interplate coupling along the mexican subduction interface: Relationships with long-term morphology and fault zone mechanical properties. *Pure and Applied Geophysics*, pages 1–20.

RUEGG, J., RUDLOFF, A., VIGNY, C., MADARIAGA, R., DE CHABALIER, J., CAMPOS, J., KAUSEL, E., BARRIENTOS, S., and DIMITROV, D. (2009). Interseismic strain accumulation measured by GPS in the seismic gap between Constitución and Concepción in Chile. *Physics of the Earth and planetary interiors*, doi:10.1016/j.pepi.2008.02.015, 175(1-2):78–85.

RUIZ, S., KLEIN, E., DEL CAMPO, F., RIVERA, E., POLI, P., MÉTOIS, M., VIGNY, C., BAEZ, J., VARGAS, G., LEYTON, F., MADARIAGA, R., and FLEITOUT, L. (2016). The Illapel Mw 8.3 earthquake triggered by deep transient slow slip. *Accepted in Seismological research letters*.

RUIZ, S., MÉTOIS, M., FUENZALIDA, A., RUIZ, J., LEYTON, F., GRANDIN, R., VIGNY, C., MADARIAGA, R., and CAMPOS, J. (2014). Intense foreshocks and a slow slip event preceded the 2014 iquique mw 8.1 earthquake. *Science*, doi: 10.1126/science.1256074, 345(6201):1165–1169.

SATO, M., ISHIKAWA, T., UJIHARA, N., YOSHIDA, S., FUJITA, M., MOCHIZUKI, M., and ASADA, A. (2011). Displacement above the hypocenter of the 2011 tohoku-oki earthquake. *Science*, doi: 10.1126/science.1207401, 332(6036):1395–1395.

SAVAGE, J. (1983). A dislocation model of strain accumulation and release at a subduction zone. *Journal of Geophysical Research-Solid Earth*, doi: 10.1029/JB088iB06p04984, 88(B6).

SCHURR, B., ASCH, G., HAINZL, S., BEDFORD, J., HOECHNER, A., PALO, M., WANG, R., MORENO, M., BARTSCH, M., ZHANG, Y., ET AL. (2014). Gradual unlocking of plate boundary controlled initiation of the 2014 Iquique earthquake. *Nature*.

SIMONS, M., MINSON, S. E., SLADEN, A., ORTEGA, F., JIANG, J., OWEN, S. E., MENG, L., AMPUERO, J., WEI, S., CHU, R., ET AL. (2011). The 2011 Magnitude 9.0 Tohoku-Oki earthquake: Mosaicking the megathrust from seconds to centuries. *science*, doi: 10.1126/science.1206731, 332(6036):1421–1425.

SOBIESIAK, M., MEYER, U., SCHMIDT, S., GÖTZE, H.-J., and KRAWCZYK, C. (2007). Asperity generating upper crustal sources revealed by b value and isostatic residual anomaly grids in the area of antofagasta, Chile. *Journal of Geophysical Research: Solid Earth*, doi: 10.1029/2006JB004796, 112(B12).

775 SONG, T. and SIMONS, M. (2003). Large trench-parallel gravity variations predict seismogenic
776 behavior in subduction zones. *Science*, doi: 10.1126/science.1085557, 301(5633):630–633.

777 TASSARA, A., GOTZE, H., SCHMIDT, S., and HACKNEY, R. (2006). Three-dimensional
778 density model of the Nazca plate and the Andean continental margin. *Journal of Geophysical*
779 *Research-Solid Earth*, doi: 10.1029/2005JB003976, 111(B9).

780 THIERER, P., FLUEH, E., KOPP, H., TILMANN, F., COMTE, D., and CONTRERAS, S.
781 (2005). Local earthquake monitoring offshore valparaiso, Chile. *N. Jb. Geol. Paläont. Abh*,
782 236(1/2):173–183.

783 TRUBIENKO, O., FLEITOUT, L., GARAUD, J., and VIGNY, C. (2013). Interpretation of in-
784 terseismic deformations and the seismic cycle associated with large subduction earthquakes.
785 *Tectonophysics*, doi:10.1016/j.tecto.2012.12.027, 589:126–141.

786 VALLEE, M., NOCQUET, J., BATTAGLIA, J., FONT, Y., SEGOVIA, M., REGNIER, M.,
787 MOTHES, P., JARRIN, P., CISNEROS, D., VACA, S., ET AL. (2013). Intense interface seis-
788 micity triggered by a shallow slow slip event in the central ecuador subduction zone. *Journal*
789 *of Geophysical Research: Solid Earth*, doi: 10.1002/jgrb.50216, 118(6):2965–2981.

790 VARGAS, G., KLINGER, Y., ROCKWELL, T., FORMAN, S., REBOLLEDO, S., BAIZE, S.,
791 LACASSIN, R., and ARMIJO, R. (2014). Probing large intraplate earthquakes at the west
792 flank of the Andes. *Geology*, doi: 10.1130/G35741.1 , 42(12):1083–1086.

793 VERGNOLLE, M., WALPERSDORF, A., KOSTOGLODOV, V., TREGONING, P., SANTIAGO, J.,
794 COTTE, N., and FRANCO, S. (2010). Slow slip events in Mexico revised from the processing

795 of 11 year gps observations. *Journal of Geophysical Research: Solid Earth (1978–2012)*, doi:
796 10.1029/2009JB006852, 115(B8).

797 VIGNY, C., RUDLOFF, A., RUEGG, J., MADARIAGA, R., CAMPOS, J., and ALVAREZ, M.
798 (2009). Upper plate deformation measured by GPS in the Coquimbo Gap, Chile. *Physics of*
799 *the Earth and Planetary Interiors*, doi:10.1016/j.pepi.2008.02.013, 175(1-2):86–95.

800 VIGNY, C., SOCQUET, A., PEYRAT, S., RUEGG, J.-C., MÉTOIS, M., MADARIAGA, R., MOR-
801 VAN, S., LANCIERI, M., LACASSIN, R., CAMPOS, J., CARRIZO, D., BEJAR-PIZARRO, M.,
802 BARRIENTOS, S., ARMIJO, R., ARANDA, C., VALDERAS-BERMEJO, M.-C., ORTEGA,
803 I., BONDOUX, F., BAIZE, S., LYON-CAEN, H., PAVEZ, A., VILOTTE, J. P., BEVIS, M.,
804 BROOKS, B., SMALLEY, R., PARRA, H., BAEZ, J.-C., BLANCO, M., CIMBARO, S., and
805 KENDRICK, E. (2011). The 2010 Mw 8.8 Maule megathrust earthquake of Central Chile,
806 monitored by GPS. *Science*, doi: 10.1126/science.1204132, 332(6036):1417–21.

807 WALLACE, L., BEAVAN, J., MCCAFFREY, R., and DARBY, D. (2004). Subduction zone cou-
808 pling and tectonic block rotations in the North Island, New Zealand. *Journal of Geophysical*
809 *Research*, doi: 10.1029/2004JB003241, 109(B12):B12406.

810 WANG, K. and BILEK, S. L. (2014). Invited review paper: Fault creep caused by subduction
811 of rough seafloor relief. *Tectonophysics*, doi:10.1016/j.tecto.2013.11.024, 610:1–24.

812 YE, L., LAY, T., KANAMORI, H., and KOPER, K. (2015). Rapidly estimated seismic source
813 parameters for the 16 september 2015 Illapel, Chile M w 8.3 earthquake. *Pure and Applied*
814 *Geophysics*, pages 1–12.

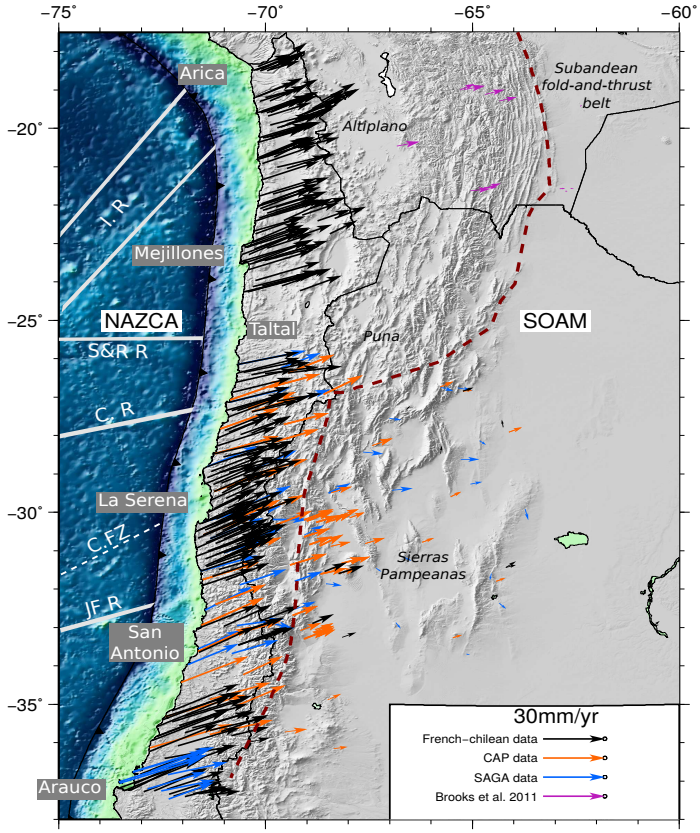

Figure 1: Combined horizontal velocity field from continuous and campaign GPS measurements plotted relative to stable South America (defined by NNR-Nuvel1A (DEMETS et al., 1994)). CAP is the name of the US experiment (BROOKS et al., 2003; BEVIS et al., 1999); SAGA is the GFZ experiment (KLOTZ et al., 2001; KHAZARADZE and KLOTZ, 2003). Dashed brow line : rough border of the eastern edge of the Andean sliver. White lines : major bathymetric features of the Nazca plate (HOFs). I.R Iquique Ridge; S&R R. Sala y Gomez Ridge (or Taltal ridge); C.R. Copiapo Ridge; C.FZ Challenger Fracture Zone; JF.R Juan Fernandez Ridge.

815 YOSHIOKA, S., WANG, K., and MAZZOTTI, S. (2005). Interseismic locking of the plate

816 interface in the Northern Cascadia subduction zone, inferred from inversion of GPS data.

817 *Earth and Planetary Science Letters*, doi:10.1016/j.epsl.2004.12.018, 231(3):239–247.

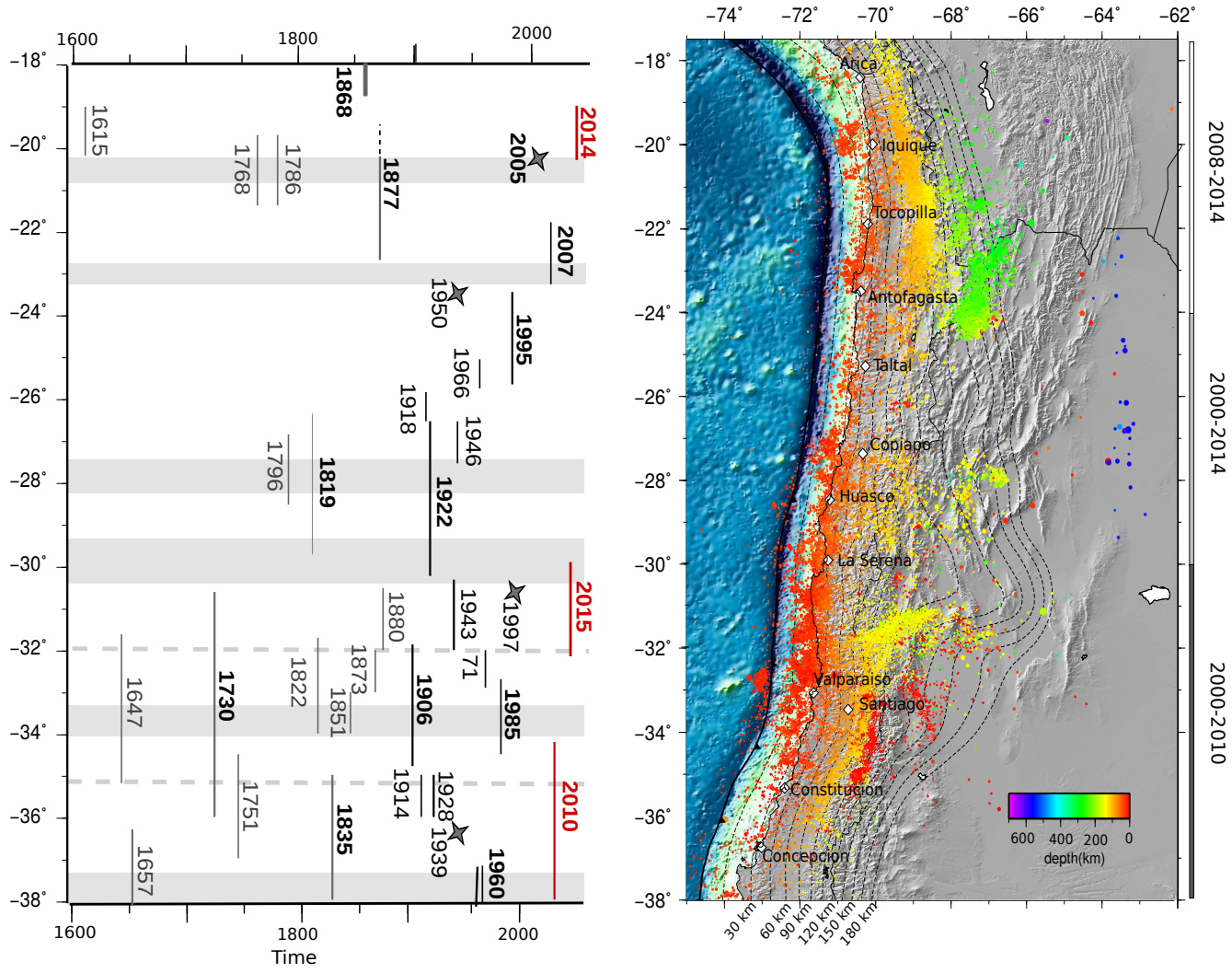

Figure 2: Left : estimated extend of large historical or instrumental ruptures along the Chilean margin adapted from MÉTOIS et al. (2012). Grey stars mark major intra-slab events. The recent Mw>8 earthquakes are indicated in red. Gray shaded area corresponds to LCZ defined in Fig.3. Right : seismicity recorded by the Centro Sismologico Chileno (CSN) during interseismic period, color-coded depending on the event's depth. Three zones have been defined to avoid including aftershocks and preshocks associated to major events : (i) in North Chile, we plot the seismicity from 2008 to january 2014, i.e. between the Tocopilla and Iquique earthquakes; (ii) in Central Chile, we plot the seismicity on the entire 2000-2014 period; (iii) in South-Central Chile, we selected events that occurred between 2000 and 2010, i.e. before the Maule earthquake.

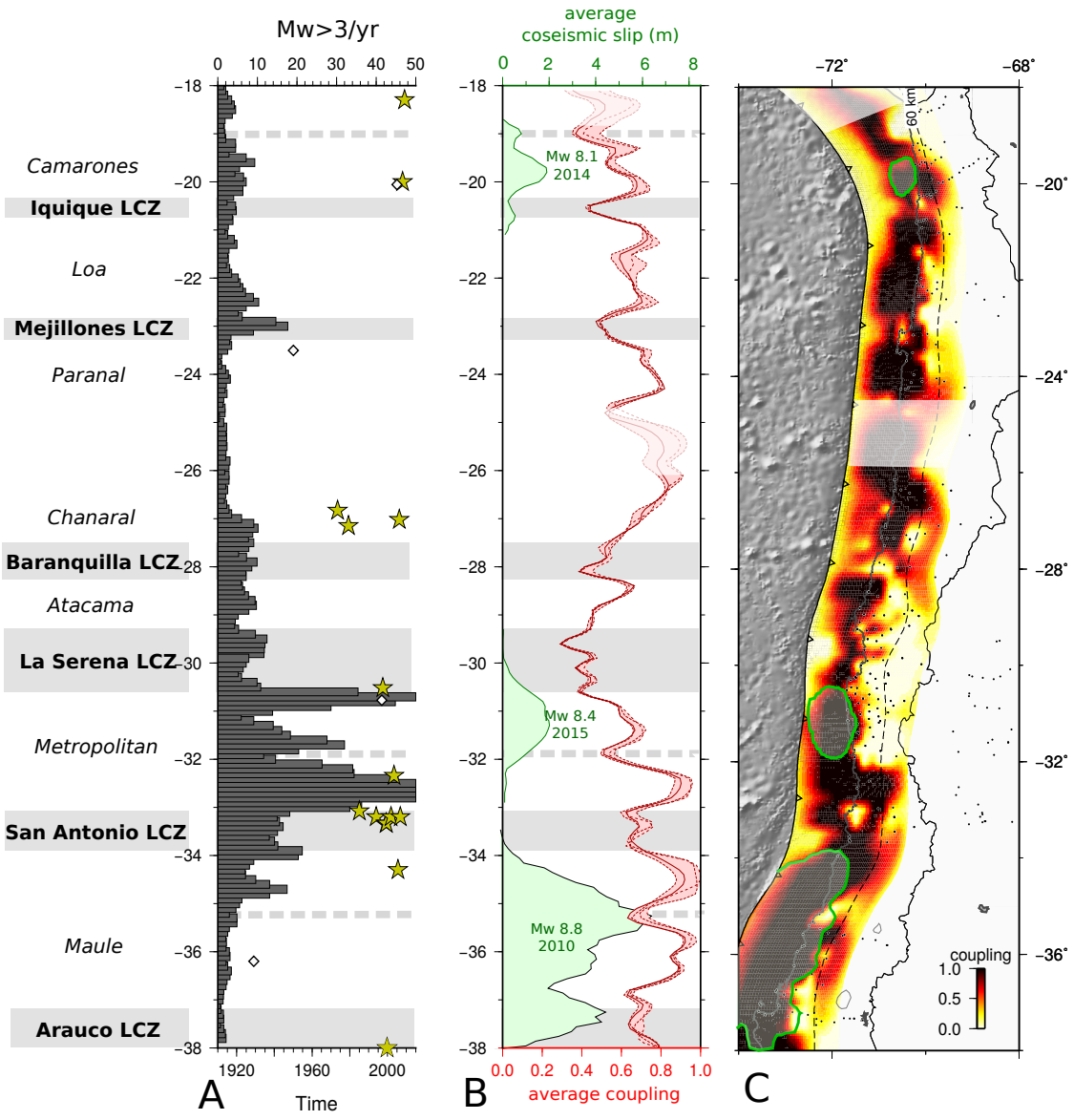

Figure 3: A- Histogram depicts the rate of Mw>3 earthquakes registered by the CSN catalogue during the interseismic period defined for each zone (see Fig.2) on the subduction interface, on 0.2° of latitude sliding windows. Stars are swarm-like sequences detected by HOLTKAMP et al. (2011) depending on their occurrence date. Swarms located in the Iquique LCZ and Camarones segment are from RUIZ et al. (2014). Empty squares are significant intraplate earthquakes. B- Red curve : variations of the average coupling coefficient on the first 60 km of depth calculated on 0.2° of latitude sliding windows for our best-models including an Andean sliver motion. Dashed pink curves are alternative models with different smoothing options that fit the data with nRMS better than 2 (see supplementary figure 6) : the pink shaded envelope around our best-model stands for the variability of the coupling along strike. Green curves : coseismic distribution for Maule (VIGNY et al., 2011), Iquique (LAY et al., 2014) and Illapel earthquakes (RUIZ et al., 2016). Gray shaded area stand for the identified Low Coupling Zones (LCZs) and associated high coupling segments that are named on the left. The apparent decrease in the average coupling North of 30°S is considered as an artifact of the Andean sliver motion (see section 5.2). C- Best coupling distribution obtained inverting for Andean sliver motion and coupling amount simultaneously. The rupture zones for the three major earthquakes are indicated as green ellipses. White shaded areas are zones where we lack resolution.

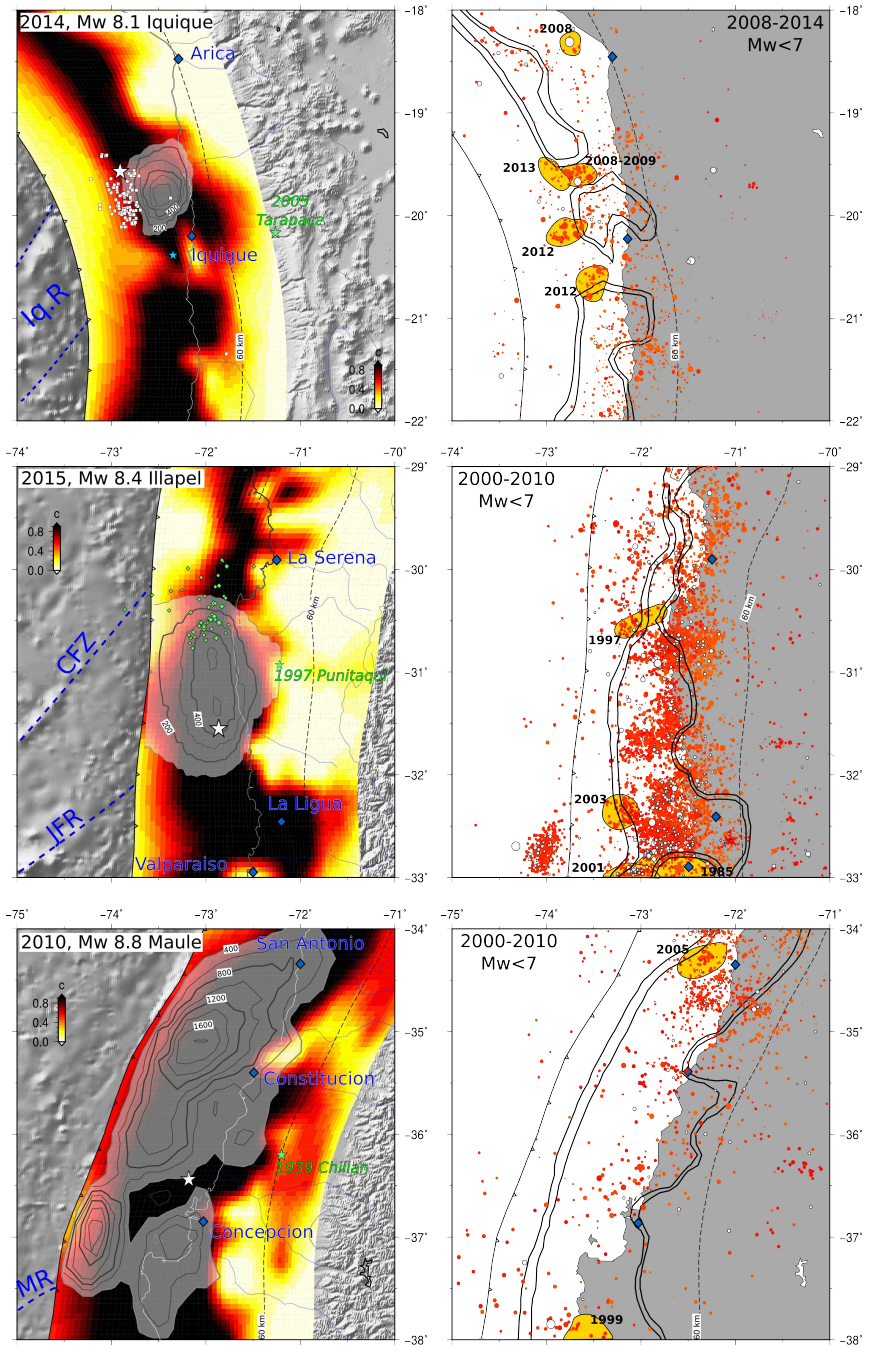

Figure 4: Left : Coupling maps (color coded) versus coseismic slip distributions (gray shaded contours in cm) for the last three major Chilean earthquakes (epicenters are marked by white stars). From top to bottom : Iquique area, white squares are pre-seismic swarm event in the month before the main shock, green star is the 2005, Tarapacá intraslab earthquake epicenter, blue star is the Mw 6.7 Iquique aftershock; Illapel area, green squares show the seismicity associated to the 1997 swarm following the Punitaqui intraslab earthquake (green star); Maule area, green star is the epicenter of the 1939 Chillan intraslab earthquake. Right : interseismic background seismicity in the shallow part of the subduction zone (shallower than 60 km depth) for each region (red dots) together with 80% and 90% coupling contours. White dots are events identified as mainshock after a declustering procedure following GARDNER and KNOPOFF (1974). Yellow areas : extend of swarm sequences identified by HOLTKAMP et al. (2011) South and Central Chile, and RUIZ et al. (2014) for North Chile.

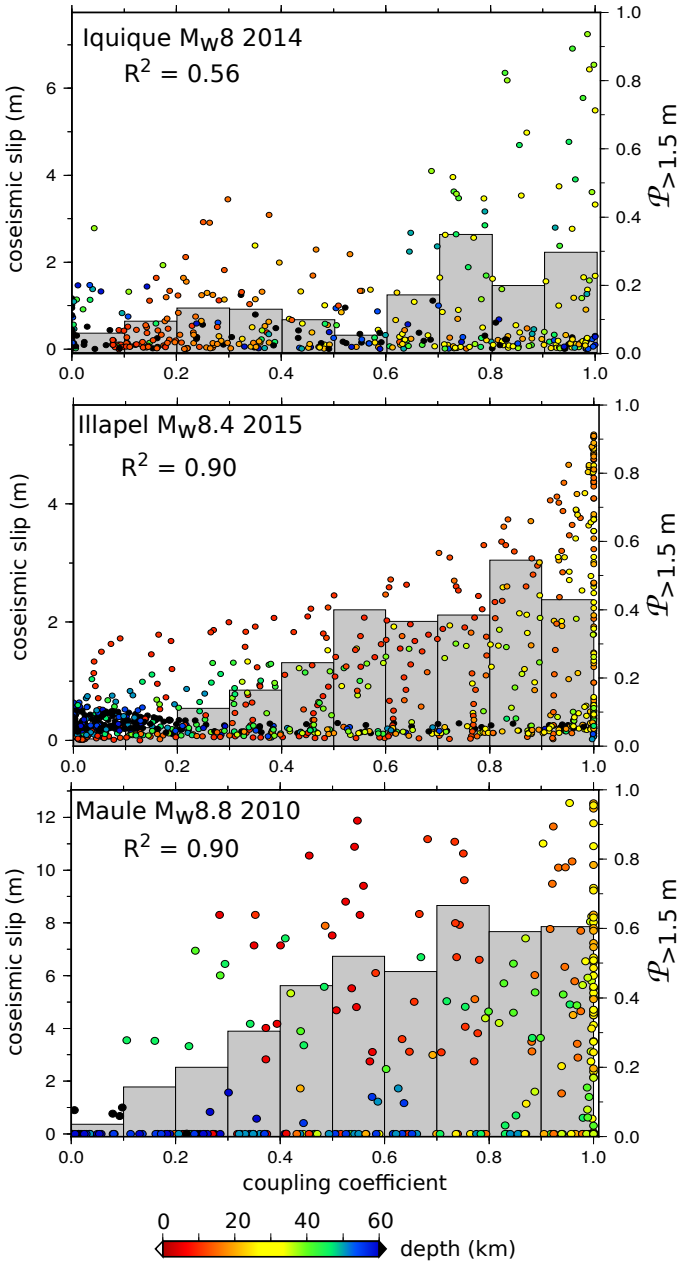

Figure 5: Correlation between coseismic slip amount and prevailing interseismic coupling for the three megathrust earthquakes that stroke Chile since 2010. From top to bottom, case of : the Iquique Mw 8 2014, the Illapel Mw 8.4 2015 and the Maule Mw 8.8 2010 earthquakes. Coseismic slip and interseismic coupling for each subfault is represented by dots, color-coded depending on the subfault depth. The conditionnal probability of experiencing more than 1.5 meter of coseismic slip depending on the prevailing coupling amount is represented by grey histograms. R^2 is the coefficient of correlation between $P_{(>1.5m)/coupling}$ and the interseismic coupling calculated for each case.